Desalination 558 (2023) 116617

Contents lists available at ScienceDirect

Desalination

journal homepage: www.elsevier.com/locate/desal

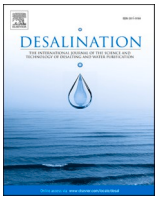

Surfactant-induced intervention in interfacial polymerization to develop highly-selective thin-film composite membrane for forward osmosis process

Xuan Zhang, Hui-Min Cui, Yu Gao, Zhi-Wei Yan, Xi Yan, Yan Chen, Xiao-Jing Guo, Wan-Zhong Lang *

The Education Ministry Key Laboratory of Resource Chemistry, Shanghai Key Laboratory of Rare Earth Functional Materials, College of Chemistry and Materials Science, Shanghai Normal University, 100 Guilin Road, Shanghai 200234, China

HIGHLIGHTS

- CTAT-induced intervention in interfacial polymerization (IP) was verified.
- Effect of CTAT contents on the formation of polyamide layer were studied.
- Incorporation of CTAT during IP leads to a uniform and dense polyamide layer.
- Resultant TFC-FO membranes show improved water flux and reduced reverse salt flux.

GRAPHICAL ABSTRACT

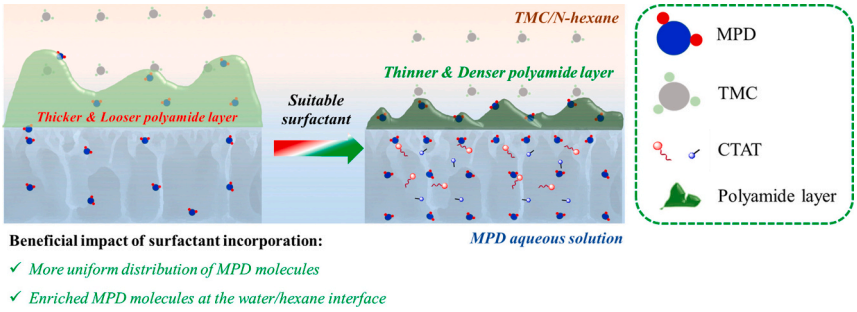

ARTICLE INFO

Keywords:
Forward osmosis (FO)
Interfacial polymerization (IP)
Surfactant
Perm-selectivity
Specific reverse salt flux

ABSTRACT

Thin-film composite (TFC) membrane capable of superior permeability contributes to the industrial implementation of forward osmosis (FO) technology, but it is plagued with some bottlenecks including the unsatisfactory selectivity. Herein, the surfactant-induced intervention in interfacial polymerization was performed by incorporating hexadecyltrimethylammonium toluene-p-sulphonate (CTAT) into the amine aqueous solution for developing the highly-permeable TFC membrane with exceptional selectivity. The effect of CTAT incorporation on the physicochemical properties of polyamide (PA) layer was systemically investigated by conventional characterizations, so as to unravel the mechanism for the improved performance of resultant TFC-FO membrane. Besides, three typical surfactants of Tween 80, sodium dodecyl sulfate (SDS) and hexadecyltrimethylammonium chloride (CTAC) were also introduced and studied contrastively for comparison. Amongst the fabricated membranes, the optimized TFC-CTAT membrane achieves the improved water fluxes (J_V) of 31.8 and 21.7 $L{\cdot}m^{-2}{\cdot}h^{-1}$ accompanied with the reduced specific reverse salt fluxes (J_S/J_V) of 0.05 and 0.04 $g{\cdot}L^{-1}$ in active layer facing the draw solution (AL-DS) and active layer facing the feed solution (AL-FS) orientations respectively, using 1 M NaCl solution and deionized water as draw and feed solutions. Therefore, this work provides a new perspective for constructing TFC-FO membrane with high perm-selectivity by employing suitable surfactant at the relatively low concentrations.

* Corresponding author.
E-mail address: wzlang@shnu.edu.cn (W.-Z. Lang).

https://doi.org/10.1016/j.desal.2023.116617
Received 24 October 2022; Received in revised form 23 March 2023; Accepted 9 April 2023
Available online 14 April 2023

Nomenclature

Abbreviations

TFC membrane	thin-film composite membrane
FO	forward osmosis
CMC	critical micelle concentration
NIPs	non-solvent induced phase separation
CTAT	hexadecyltrimethylammonium toluene-p-sulphonate
SDS	sodium dodecyl sulfate
CTAC	hexadecyltrimethylammonium chloride
PA	polyamide
FESEM	field emission scanning electron microscopy
AFM	atomic-force microscopy
ATR-FTIR	attenuated total reflectance Fourier transform infrared analysis
WCA	water contact angle

Symbols

Ra	average surface roughness (nm)
Rq	root mean square roughness (nm)
A	water permeability coefficient ($L{\cdot}m^{-2}{\cdot}h^{-1}{\cdot}bar^{-1}$)
B	salt permeability coefficient ($L{\cdot}m^{-2}{\cdot}h^{-1}$)
V_d	the volume of draw solution (L)
V_f	the volume of feed solution (L)
$C_f{}^0$	the initial concentration of feed solution ($mol{\cdot}L^{-1}$)
$C_f{}^1$	the final concentration of feed solution ($mol{\cdot}L^{-1}$)
$C_d{}^0$	the initial concentration of feed solution ($mol{\cdot}L^{-1}$)
$C_d{}^1$	the final concentration of feed solution ($mol{\cdot}L^{-1}$)
R	the rejection of solute (%)
J_W	pure water flux ($L{\cdot}m^{-2}{\cdot}h^{-1}{\cdot}bar^{-1}$)
A_m	the effective membrane area (m^2)
t	the operation time (h)
C_f	the salt concentration of feed solution ($mol{\cdot}L^{-1}$)
C_P	the salt concentration of the permeate solution ($mol{\cdot}L^{-1}$)
C_0	the initial salt concentration ($mol{\cdot}L^{-1}$)
C_1	the final salt concentration ($mol{\cdot}L^{-1}$)
V_1	the final volume during FO process (L)
V_0	the initial volume during FO process (L)
J_V	FO water flux (LMH)
J_S	reverse salt flux (gMH)
ΔV	the volume change of the solution (L)

1. Introduction

Forward osmosis (FO), as one of the promising membrane separation technologies, has attracted the unprecedented attention during the past decades and it has exhibited promising potential in the industrial application fields of seawater desalination, power generation, wastewater enrichment, food processing and etc., because the osmotic pressure gradient is employed as the driving force to realize the transport of water molecules from the feed solution (with low osmotic pressure) to the draw solution (with high osmotic pressure) unidirectionally [1–6]. Accordingly, FO possesses the distinct merits of low fouling propensity, low energy consumption and high recovery rate of the freshwater in comparison with those of the traditional pressure-driven membrane processes such as nanofiltration and reverse osmosis [7–9]. However, the lack of desirable FO membrane is still the main bottleneck confined its further advancement and industrial applications [10,11]. State-of-the-art approach for the preparation of FO membrane is the thin-film composite (TFC) membrane since it is capable of particular advantages including easy preparation, low-cost, outstanding separation performance and pH tolerance [12–14]. However, the typical TFC membranes fabricated by *m*-phenylenediamine (MPD) and trimesoyl chloride (TMC) are also plagued with several bottlenecks including the permeability-selectivity trade-off, high fouling tendency and poor membrane stability [15]. Accordingly, numerous researches have been performed innovatively to address above bottlenecks, such as the design of highly-permeable substrate [15–17], construction of the polyamide (PA) layer with specific architecture [18], in-situ modification and post-treatment of the PA layer [12,19–21], the employment of the functional interlayer between substrate and PA layer [22–24], development of the biomimetic FO membranes [25–28] and etc. [29]. In addition to the promoted membrane permeability and stability of resultant TFC membranes, a great challenge lies in the construction of the TFC-FO membrane with excellent selectivity which still calls for novel approaches to ameliorate, because the FO membrane with satisfactory selectivity is the critical prerequisite for reducing the chemical, energy and cost efficiency gains as well as ensuring the high quality of freshwater and in terms of the actual large-scale applications [30].

A vast number of investigations demonstrate that the in-situ regulation of the PA layer by incorporating functional components in the aqueous and/or the organic phases during the interfacial polymerization (IP) reaction process is favorable for improving the membrane selectivity by changing the reaction kinetics, altering the diffusion rate of amine monomer from the aqueous to the organic phase and/or participating in the formation of PA layer [22,31]. In comparison with the ultrafine particles [32], nano-materials [33], polymeric additives [34], co-reactants [13] and co-solvents [35,36], the incorporation of phase transfer catalyst (e. g. surfactants [37,38]) to conduct the modification of PA layer is generally economic, environmental-friendly and easy to scale-up. Several familiar surfactants of Sorbian monolaurate (Span 20) [37], sodium dodecyl sulfate (SDS) [38], cetyltrimethylammonium bromide (CTAB) [39] and cetyltrimethylammonium chloride (CTAC) [40] have been adopt and the resultant TFC-FO membranes were endowed with exceptional properties, because the incorporation of surfactants effectively reduces the surface tension of the amine aqueous solution which is favorable for the improved wettability of the substrate layer and therefore the higher adsorption amount of amine monomers [37,41]. Meanwhile, the existence of surfactants facilitates the transport of amino monomers across the water/hexane interface during the IP reaction by reducing the associated Gibbs free energy barrier, resulting in the spatially homogeneous polymerization [38]. However, the immoderate promotion of the amine monomer towards the organic phase during IP might lead to the synchronous decrease of membrane permeability and selectivity, because the stronger Marangoni effect adversely leads to the formation of the much thicker and more multilayered PA layer with defects [41]. In addition to above beneficial effect, pioneering work by Tang's group also demonstrates that the incorporation of surfactant at a certain concentration during IP process was advantageous to the stabilization of generated nanobubbles at the reaction interface, resulting in the formation of the defect-free PA layer with the apparent nanovoids structure, whereas the stabilization effect was negated and accordingly resulted in the deteriorated membrane performance, due to the excessive loading of the surfactant [42]. Generally, the added surfactants were in the form of micelle in some cases because the loading amounts were higher than their critical micelle concentrations (CMC). It might lead to the formation of linear PA molecular chains with the relatively lower crosslinking degree [31]. Moreover, the formed micelles would be washed away and left the PA layer with defects [38,43]. These factors lead to the decreased membrane selectivity inevitably. To the best of our knowledge, there still have room to further improve the selectivity of fabricated TFC-FO membrane by simply incorporating suitable surfactants with relative low concentration. Our previous work has verified

that the strengthened interaction between substrate and amine monomers effectively enhances the loading of MPD and results in the uniform and smooth PA layer with the improved selectivity, as indicated by the parameter of specific reverse salt flux (J_S/J_V) decreased from 0.84 to 0.24 g·L^{-1} [44]. Therefore, we envision that the uniform distribution of amine monomer at the interface, the accelerated kinetic reaction of interfacial polymerization might be conductive to develop the TFC-FO membrane with the superior selectivity.

In this work, hexadecyltrimethylammonium toluene-p-sulphonate (CTAT) composed of a cationic part of linear alkane chains, co-existence of the anionic part of toluene-p-sulphonate was introduced in MPD aqueous phase as additive to regulate the structure and chemical properties of resultant TFC-FO membrane with the merit described in Section 1 of the **Supporting Information** in detail. In addition to the conventional merit of the decreased surface tension by surfactant, the incorporation of CTAT may have the additional interplays including the π-π interaction between the aromatic groups of CTAT and MPD [36], the electrostatic interaction between the negatively charged sulfonic acid group and slightly charged MPD monomers [45], as well as the hydrogen bonding. There interaction might favor the enrichment and uniform distribution of MPD molecules at the water/hexane interface and the subsequently the formation of a dense, thinner and defect-free PA layer, therefore improving the perm-selectivity of the modified TFC-FO membrane. To verify above inferences, obvious changes in TFC membranes in terms of the microstructure morphology, hydrophilicity, crosslinking degree of the modified PA layer are comprehensively studied according to the membrane performance test and many conventional characterizations. Besides, three common surfactants at the optimized content were also introduced and studied contrastively for the purpose of elaborating the underlying modification mechanism. In addition to the decreased surface tension of amine solutions, this work demonstrates that the employment of surfactants with intense interaction to amine monomers could be a straightforward and simple experimental strategy for designing highly-selective TFC membrane in forward osmosis.

2. Experimental

2.1. Materials

Polyvinylidenefluoride (PVDF) flat-sheet substrates with the porosity and mean pore size of 65.4 ± 1.7 % and 34.3 ± 0.1 nm respectively, were prepared through the traditional non-solvent induced phase separation (NIPs) method in advance, as described in our previous work [46]. N-hexane (AR, ≥97.0 %) and sodium chloride (NaCl, AR, ≥99.5 %) were purchased from Shanghai Chemical Agent Company (China). Polyvinylpyrrolidone (PVP) with the molecular weight of 58 kDa, 1,3,5-benzenetricarbonyl trichloride (TMC, 98 %) and *m*-phenylenediamine (MPD, 99.5 %) were purchased from Shanghai Aladdin Chemical Agent Co. Ltd. (China). Deionized (DI) water was self-produced by a lab-scale reverse osmosis (RO) system. The surfactants of hexadecyltrimethylammonium toluene-p-sulphonate (CTAT, 98 %), Tween 80, sodium dodecyl sulfate (SDS, 99 %), hexadecyltrimethylammonium chloride (CTAC, 97 %) and other chemicals were also acquired from Shanghai Aladdin Chemical Agent Co. Ltd. (China). The chemical structures of surfactants used in this study were shown in Fig. S1 of the **Supporting Information**.

2.2. Preparation of TFC-FO membranes

The polyamide (PA) selective layer of the TFC-FO membranes was formed by the conventional interfacial polymerization (IP) reaction between the monomers of MPD and TMC atop the PVDF substrates. Briefly, MPD aqueous solutions according to the predetermined recipes were poured onto the top surface of PVDF substrate. The detailed compositions and concentrations of surfactants in MPD solutions are summarized in Table 1 respectively. After 2-min contact, the redundant MPD solution was drained off by using a rubber roller. Then, the top surface of the MPD-saturated substrate was contacted to the 0.15 wt% TMC/n-hexane solution for 1 min to accomplish the IP reaction. Finally, the as-obtained TFC membrane was stored in DI water before use. As labeled in Table 1, TFC membranes were denominated as CTAT-x, where 'x' represents the content (mg·L^{-1}) of CTAT in MPD aqueous solutions. The denotation of 'TFC-surfactant' is representative of the particular component of the surfactant employed in the amine solutions. Herein TFC-0 indicates the pristine TFC membrane since no surfactant added into the amine solution.

Table 1
Detailed composition of amine aqueous solution for the preparation of TFC-FO membranes.

Membrane code	Composition of amine aqueous solution during IP process				
	Tween 80 (mg·L^{-1})	SDS (mg·L^{-1})	CTAC (mg·L^{-1})	CTAT (mg·L^{-1})	MPD (wt%)
TFC-0 (CTAT-0)					3
CTAT-20				20	
CTAT-40				40	
CTAT-80 (TFC-CTAT)				80	
CTAT-120				120	
TFC-Tween 80	80				
TFC-SDS		80			
TFC-CTAC			80		

2.3. Characterizations

2.3.1. Membrane characterization

Attenuated total reflectance Fourier transform infrared (FTIR-7600, Lambda Scientific Pty. Ltd., Australia) and X-ray photoelectron spectroscopy (XPS, Thermo fisher Scientific K-Alpha, Germany) were employed to verify the change of chemical properties of fabricated membranes. Wide-angle X-ray diffraction (WXRD, D/Max-2000, Rigaku Reagent Co. Ltd., Japan) was also performed to calculate the inter-chain spacing distance (d-spacing) of the PA layer of fabricated TFC membranes through the Bragg's Law. The detailed information referred to our previous work [12] was described in the **Supporting Information**. The top surface and cross-sectional morphological structure of the fabricated membranes were observed by a field emission scanning electron microscopy (FESEM, S-4800, Hitachi Co., Japan). The dried membrane samples were fractured in liquid nitrogen to get a clear observation of the cross-sections. All of the samples were posted onto a copper holder and sputtered with gold before taking FESEM images. Besides. the surface roughness of all membranes was also detected by atomic-force microscopy (AFM, 5500AFM, Agilent Technologies, USA) under the tapping mode. The parameters of average surface roughness (*Ra*) and the root mean square roughness (*Rq*) are indicative to verify the roughness change of fabricated membranes. All samples were tested at room temperature with the scanning area of 3 × 3 square micrometers at a speed of 2 Hz. The water contact angle (WCA) was detected by using a Goniometer (DSA30, KRÜSS, Germany) for the purpose of evaluating the surface wettability of as-fabricated membranes. At least 3 samples with >10 testing points were measured for each TFC membrane to minimize the artificial error.

2.3.2. Other characterizations

The difference of the surface tension of amine solutions containing different surfactants was clarified by an automatic surface tension meter (BZY-1, Shanghai Hengping Instrument and meter Factory, China). The results were averaged on at least 5 parallel tests of each sample to minimize the artificial error. An UV–Vis spectrophotometer (UV-3600,

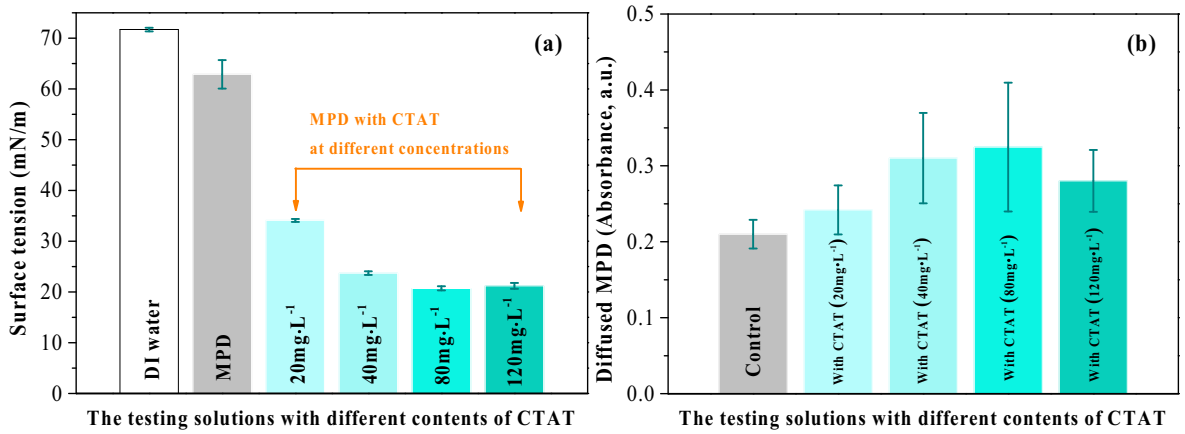

Fig. 1. (a) Effect of CTAT contents on the surface tension of the corresponding aqueous solutions, and (b) effect of CTAT incorporation on the diffusion of MPD into the organic phase (n-hexane).

Shimadzu, Japan) was employed to probe the change of the MPD diffusion rate according to the pioneering work [42]. Specifically, 0.5 mL MPD solution at the concentration of 3 wt% was injected into the bottom side of the cuvette, and 3 mL of n-hexane was gently supplemented atop the MPD solution. After 1 min, the MPD diffusion from the aqueous to the hexane phase could be recorded by UV spectrophotometer at the wavelength of 294 nm, since the MPD concentration in the hexane phase is proportional to the absorbance intensity. Similarly, MPD solutions with surfactants (referred to Table 1) were also parallelly tested.

2.4. Performance evaluation of TFC-FO membranes

2.4.1. Intrinsic separation properties

A lab-scale cross-flow filtration equipment was employed to conduct the filtration test for the measurement of water permeability coefficient (A, $L{\cdot}m^{-2}{\cdot}h^{-1}{\cdot}bar^{-1}$) according to Eq. (1). The nascent TFC membrane was pre-pressured at 2.0 bar for 1 h, followed by performing the tests at 1.0 bar [17],

$$A = \Delta V / (A_m \bullet \Delta P \bullet t) \tag{1}$$

where ΔV is the volume (L) of collected permeate solution during the testing period time (t). The parameters of ΔP and A_m represent the applied hydraulic pressure (bar) and effective membrane area (m^2) respectively.

The solute permeability coefficient (B) was examined by a lab-scale FO devices in PRO mode (active layer facing the draw solution orientation, AL-DS), using 1 M NaCl aqueous solution and DI water as the draw and feed solutions respectively. Under the assumption that the concentration of the draw solution was constant during the testing period time, the value of B was calculated by Eq. (2) according to the previous work [47],

$$B = \frac{1}{A_m t\left(\frac{1}{V_d} + \frac{1}{V_f}\right)} ln\left(\frac{C_d^0 - C_f^0}{C_d^1 - C_f^1}\right) \tag{2}$$

where V_d and V_f represent the volumes (L) of the draw and feed solutions respectively. The change of NaCl concentration in the draw (C_d) and feed (C_f) solutions as a function of testing time (t) were measured using a conductivity meter (FE38 Standard, Mettler Toledo, Switzerland).

2.4.2. FO performance

The FO test was performed under both of the active layer faced the feed solution (AL-FS, FO mode) and active layer faced the draw solution (AL-DS, PRO mode) orientations at 25 ± 1 °C, using the 1 M NaCl aqueous solution and DI water as the draw and feed solutions respectively. The detailed operation was described in our previous works [17,44]. The parameters of water flux (J_V, $L{\cdot}m^{-2}{\cdot}h^{-1}$, abbreviated as LMH) and reverse salt flux (J_S, $g{\cdot}m^{-2}{\cdot}h^{-1}$, abbreviated as gMH) determined by Eqs. (3) and (4) were used to evaluate the FO performance of fabricated TFC membranes [48],

$$J_V = \Delta V' / (A_m \bullet \Delta t) \tag{3}$$

$$J_S = \Delta(C_t V_t) / (A_m \bullet \Delta t) \tag{4}$$

where ΔV' is the volume change resulted from the water delivery from the feed solution to the draw solution at the determined time intervals (Δt). The parameters of C_t and V_t stand for the concentration and volume of the solution at the testing points. Specifically noted that the FO tests of each membrane sample were lasted for over 3 h for stabilization. The NaCl rejection (R) of TFC membrane in PRO mode was measured by detecting the concentration change of the feed and permeate solutions during the FO tests, and calculated by Eqs. (5) and (6) [47],

$$R = (C_f - C_p) / C_f \times 100\% \tag{5}$$

$$C_p = (C_t V_t - C_0 V_0) / (V_t - V_0) \tag{6}$$

where C_0 and V_0 represent the initial concentration and volume of draw solution respectively.

3. Results and discussion

3.1. Effect of CTAT content on the surface tension and diffusion behavior of MPD solutions

To verify the change of the physicochemical properties on the formation of PA selective layer, the effect of CTAT incorporation on the surface tension and diffusion behavior of MPD solutions was evaluated in advance. It can be seen from Fig. 1 (a) that the incorporation of surfactants in MPD solution effectively decreases the surface tension of aqueous solutions, which correspondingly favors the higher stocking and better distribution of the amine solution on membrane substrate, resulting in the increased quantity of amine in the reaction zone accordingly [49], and therefore the facilitated transport of MPD into the organic phase. It could be demonstrated by the results in Fig. 1 (b), since that the diffusion of MPD molecules was accelerated gradually with the increase of the CTAT content. However, as the content of CTAT increase up to 120 $mg{\cdot}L^{-1}$, the surface tension of MPD-CTAT aqueous solution could not further decrease and reach the platform, but the excess loading

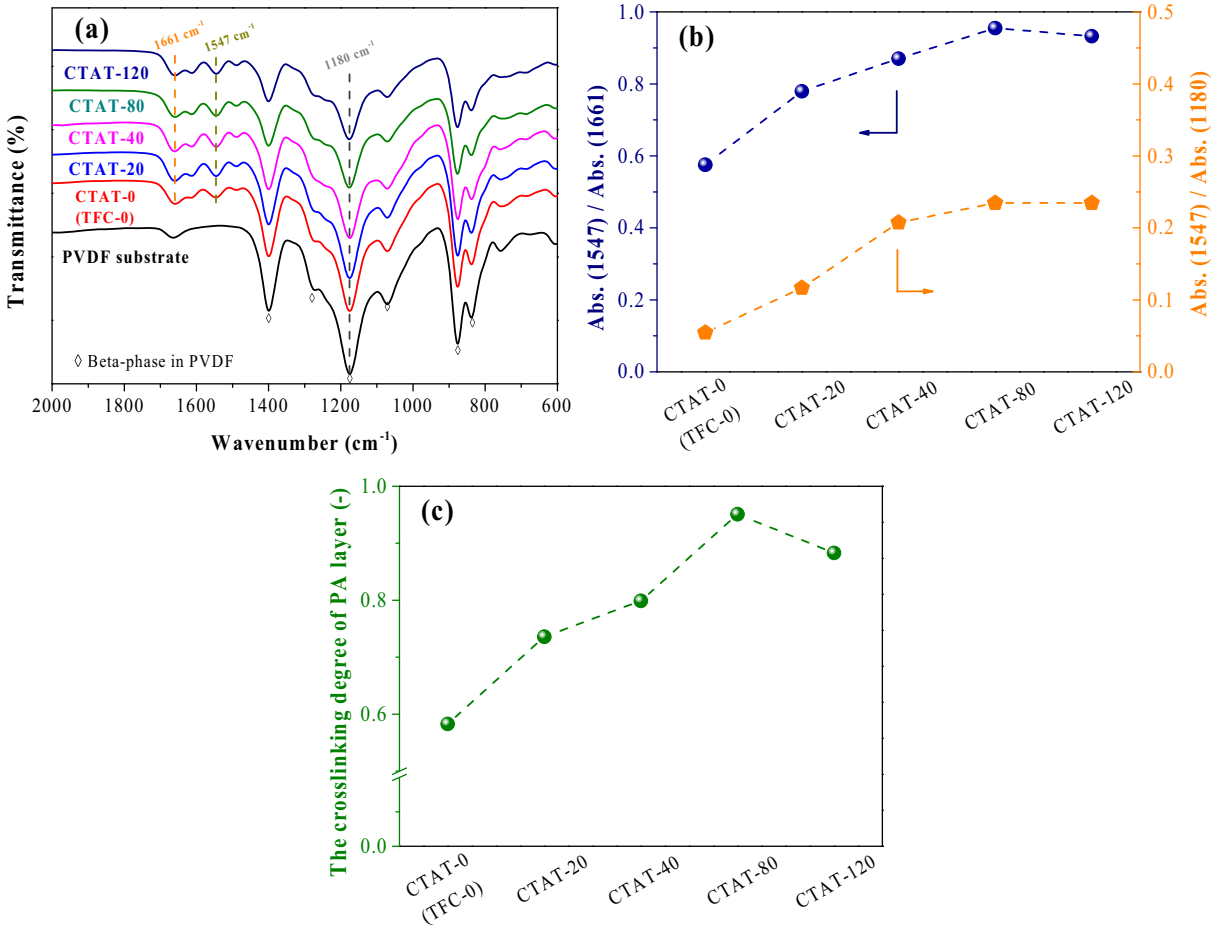

Fig. 2. (a) ATR-FTIR spectra of PVDF substrate and fabricated TFC membranes with different contents of CTAT in MPD solution, (b) the corresponding absorbance ratios of Abs. (-CONH-) / Abs. (-COOH) and Abs. (-CONH-) / Abs. (C–F) and (c) the calculated values of the crosslinking degree of the formed PA layer based on the element ratios of O/N by XPS analysis.

of CTAT adversely leads to the decrease of MPD diffusion to some extent. Such decrease of the diffusion rate might be due to the hindered effect by surfactants as a result of the combined interactions of the electrostatic interaction, π-π interaction and hydrogen bonding [37,50]. In a conclusion, the kinetics of MPD diffusion from the aqueous to the organic phase were determined by the two combined factors of the surface tension and the interaction between the surfactant and MPD.

3.2. *Effect of CTAT content on physicochemical properties of resultant PA layer*

ATR-FTIR technique was employed to detect the change of chemical properties of as-fabricated TFC membranes. As depicted in Fig. 2 (a), characteristic peaks at 1402, 1275, 1180, 1075, 876 and 841 cm^{-1} ascribed to the dominating beta-phase of PVDF were revealed for all membrane spectra, which is also in accordance with those observation in our previous works [17,44,51]. In addition to the beta-phase of PVDF, the peaks with relatively low intensity at 614, 760 and 975 cm^{-1} correspond to the alpha-phase of PVDF [52]. The adsorption peaks and their assignments of PVDF membranes were specified and the detailed information was shown in Table S1 of the **Supporting Information**. In terms of the TFC membranes with PA layer, the appearance of intensive peaks at 1661, 1610 and 1547 cm^{-1} are observed, corresponded to the C═O stretching vibration of amide I, aromatic ring breathing and in-plane C—N stretching vibration of amide II [17,31,35]. In comparison with the spectrum of PVDF substrate, above evident change in membrane spectra demonstrates the successful growth of PA layer atop the substrate.

Moreover, it also can be surveyed that the intensity of characteristic peaks of PA gradually strengthened with an increase in the content of incorporated CTAT in MPD solution, accompanied with the attenuated intensity of those characteristic peaks for PVDF. Since the effective detection depth of ATR-FTIR technique reaches to about 1 μm, the characteristic features of PA layer and PVDF substrate were both revealed in the spectra [53]. To further discuss the chemical property of PA layer, the comparison of the absorbance at the specific wavenumbers was performed since FTIR is considered as a semi-quantitative approach to evaluate the crosslinking degree of resultant PA layer as demonstrated by previous works [12,35,44,54]. Because the formation of C—N bond is solely resulted from the crosslinking reaction between MPD and TMC and all the carbonyl groups come from TMC monomer, the absorbance ratio of the crosslinked part of PA at 1547 cm^{-1} and amide I at 1661 cm^{-1} (denoted as Abs. (1547) / Abs. (1661)) is indicative to the crosslinking degree of resultant TFC membranes [44,55]. Furthermore, the absorbance ratio of crosslinked part of PA at 1547 cm^{-1} to that of PVDF at 1180 cm^{-1} (denoted as Abs. (1547) / Abs. (1180)) could be employed to represent the amount of PA polymer because the absorption of C—F bond originated from the PVDF substrate can be considered as an invariant [35]. The results of the calculated absorbance ratios of Abs. (1547) / Abs. (1661) and Abs. (1547) / Abs. (1180) are shown in Fig. 2 (b) and the detailed information was summarized in Section S3 of the **Supporting Information**. The results show that the ratio of Abs. (1547) / Abs. (1661) exhibits an up-and-down trend, demonstrating that the incorporation of CTAT in MPD aqueous solution is favorable for

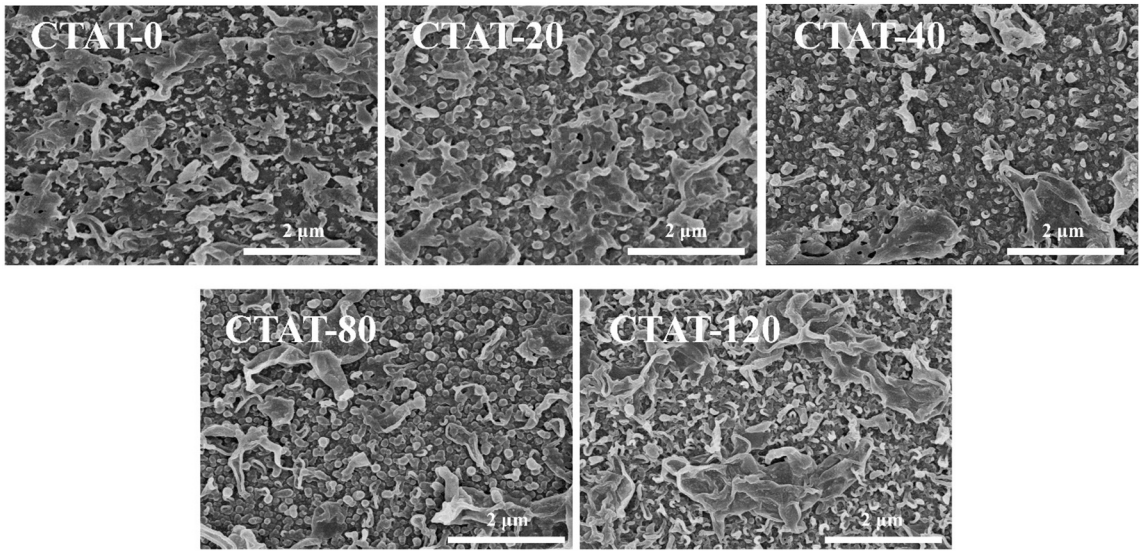

Fig. 3. Top surface morphologies of as-fabricated TFC membranes as a function of the increased concentration of CTAT incorporated to amine solution. The scale bar in the picture represents the length of 2.0 μm.

enhancing the crosslinking degree of resultant PA layer. Besides, the value of Abs. (1547) / Abs. (1180) rises from 0.05 of the pristine TFC membrane to 0.20 of CTAT-40 obviously and then slightly increases until reaching the platform of around 0.23 for CTAT-80 and CTAT-120 membranes. Moreover, results in Fig. S2 of the **Supporting Information** demonstrate that the d-spacings of the modified TFC membranes range from 5.00 to 5.38 Å, much lower than that (5.72 Å) of the pristine TFC membrane. The decrease of the d-spacing of the PA layer is highly consistent with the increase of the crosslinking degree of resultant TFC membranes. Besides, results in Fig. 2 (c) also demonstrate that the TFC membranes with the incorporation of CTAT in IP process exhibit the overall higher crosslinking degree of resultant PA layer than that of the pristine TFC membrane. And the crosslinking degree of fabricated TFC membranes also show an up-and-down trend with the increase in the CTAT content, which is roughly consistent with the results of ATR-FTIR characterization. Above results not only confirm that more PA polymer was immobilized on the top surface of PVDF substrate with the increase of CTAT content incorporated in MPD during the IP process, but also verifies that the addition of CTAT in amine solution during interfacial polymerization is beneficial for the formation of a more compacted PA layer as a result of the higher crosslinking degree.

The top surface morphology of as-fabricated TFC membranes characterized by SEM are shown in Fig. 3. Generally, all the TFC membranes roughly show the typical 'ridge-and-valley' surface features, originated from the migration of amino monomer (MPD) towards to the organic phase and further crosslinked by TMC through the IP reaction as widely reported [41]. It can be found that the pristine membrane of CTAT-0 has a relatively smooth PA surface, which is composed of the nodular structure in a relatively lower density and the irregular leaf-like structure closely sticked atop the nodular surface, probably due to the inadequate adsorption and uneven distribution of MPD monomers resulted from the relatively poor hydrophilicity (with the WCA of 84° [46]) of PVDF substrate. The boundary between these two surface configurations is not obvious. With the content of CTAT increases from 0 to 80 mg·L^{-1} in the MPD solutions, the nodular-like structure gradually dominates the top surface with the larger dimensions, accompanied

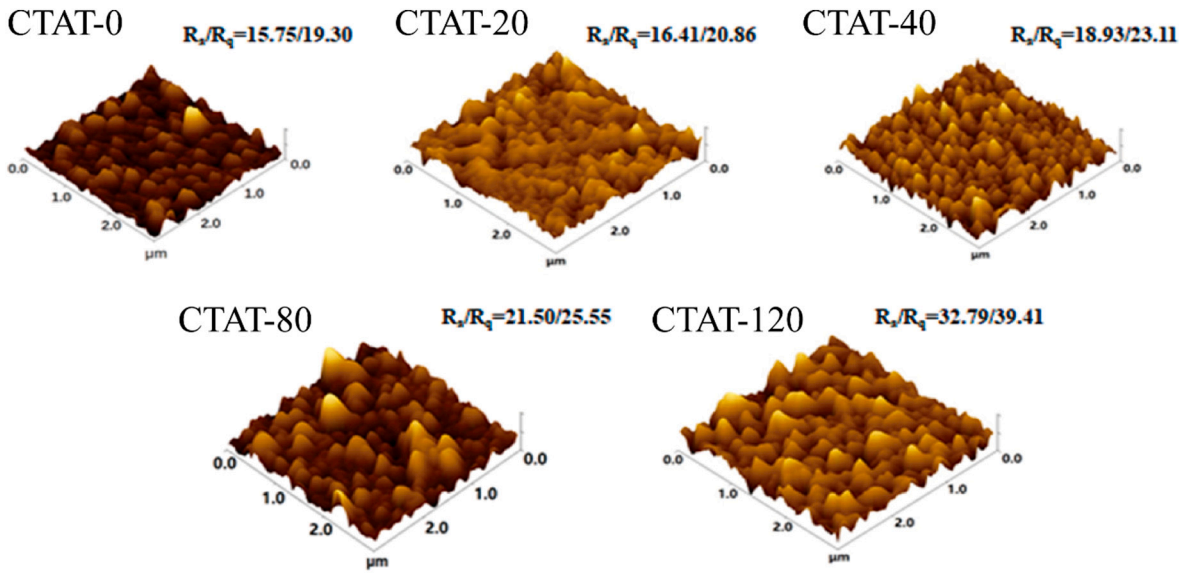

Fig. 4. AFM images of the TFC FO membranes with different concentrations of CTAT incorporated in aqueous solution.

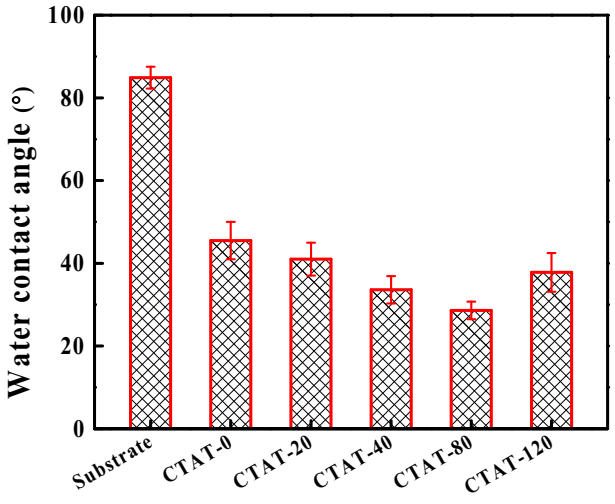

Fig. 5. Water contact angles of as-fabricated membranes.

with the randomly distributed leaf-like structure in a larger and rougher configuration. Such obvious change should be reasonably ascribed to the change of surface tension of amine solutions and the MPD diffusion rate brought by the incorporation of CTAT. As discussed before, the reduced surface tension (Fig. 1 (a)) resulted from the incorporation of CTAT favors the higher stocking and better distribution of the amine solution on membrane substrate, resulting in the increased quantity of amine in the reaction zone [49]. Accordingly, the MPD monomers not only shows the higher tendency for the migration from the aqueous to the organic phase, but also be inclined to spread to the deep region of the organic phase. Therefore, at the initial stage of the IP reaction, the adequate MPD monomers favors the uniform and intense reaction, thereby producing a relatively dense incipient PA layer at the water-organic interface. Meanwhile, the spread of MPD into the deep region of the organic phase induces the formation of PA fragments above the nascent PA layer. Afterwards, the accelerated migration of MPD towards the organic phase (Fig. 1 (b)) intensifies the IP reaction and consequently shortens the reaction time for the MPD solution incorporated with CTAT, which could hardly bring any obvious change of the nascent smooth PA layer. Meanwhile, the PA fragments formed above the dense PA layer ultimately form the loosely aggregated, roof-like structure atop the dense PA layer [56]. In comparison with CTAT-80, the thicker and rougher PA layer of CTAT-120 might be ascribed to the reduced MPD diffusion as a result of the interaction between CTAT and MPD, since it prolongs the IP reaction process and left enough time for the growth of the multi-layer PA layer as well as a more pronounced leaf-like structure above the nodular like PA surface. Consequently, the membrane of CTAT-120 exhibits the larger thickness of PA layer. In addition, as inspired by the pioneering work by Tang's group [42], the incorporation of CATA might also contributes to the larger nanovoids structure by mitigating the dissolution and escape of the nanobubbles and therefore the formation of the leaf-like structure in a relatively larger dimension.

AFM images of the fabricated TFC membranes are depicted in Fig. 4. In comparison with the relatively smooth surface of the pristine TFC membrane, the top surfaces for the modified TFC as a function of the concentration of CTAT incorporated to the amino solution become rougher, as indicated by the gradually increased value of the surface roughness. Even though the incorporation of CTAT intensifies the interfacial polymerization reaction in the initial stage by decreasing the surface tension and leads to the formation of a denser and more compact nascent PA layer with the relatively smooth surface, the formation of the PA fragments in relative larger dimensions might be responsible for the rougher surface of PA.

Based on above results and analysis, the changes of the chemical properties and the surface configuration have direct impact on the

Table 2
Intrinsic separation properties of CTAT-modified TFC FO membranes.

Membrane No.	Rejection of NaCl (%)	A ($L{\cdot}m^{-2}{\cdot}h^{-1}{\cdot}bar^{-1}$)	B ($L{\cdot}m^{-2}{\cdot}h^{-1}$)	B/A (bar)
TFC-0	85.59 ± 4.00	0.71 ± 0.08	0.49 ± 0.01	0.69 ± 0.01
CTAT-20	89.93 ± 1.56	1.59 ± 0.24	0.56 ± 0.18	0.35 ± 0.07
CTAT-40	92.59 ± 1.86	2.14 ± 0.21	0.78 ± 0.15	0.36 ± 0.07
CTAT-80	96.01 ± 1.67	3.11 ± 0.14	0.94 ± 0.14	0.30 ± 0.04
CTAT-120	95.43 ± 2.13	2.75 ± 0.12	0.88 ± 0.23	0.32 ± 0.08

hydrophilicity of membranes. Accordingly, the water contact angles of as-fabricated TFC membranes were further measured and the results of the WCA values are shown in Fig. 5. In comparison with the high WCA of 84° for PVDF substrate, TFC membranes exhibit the lower WCA values, demonstrating again the immobilization of relatively hydrophilic PA layer atop the substrate. Besides, the modified TFC membranes show the gradually reduced trend of WCA values except the membrane of CTAT-120. The gradually reduced WCA could be ascribed to the hydrophilic membrane surface with the higher surface roughness according to the Wenzel model [57] and herein the surface roughness might make more contribution to the decrease of WCA. For CTAT-120 membrane with the rougher surface and the relatively lower crosslinking degree of the PA, the water contact angle should be lower than that of CTAT-80 in theory. Herein, the abnormal WCA of CTAT-120 might be ascribed to the influence that the roughness can increase WCA if air remains trapped between the solid surface rugosities and the liquid droplet as reported by others [58,59]. The gradually reduced WCA demonstrates the enhanced membrane hydrophilicity which is favorable for the adsorption and the subsequent transport of water droplets across the membrane, and

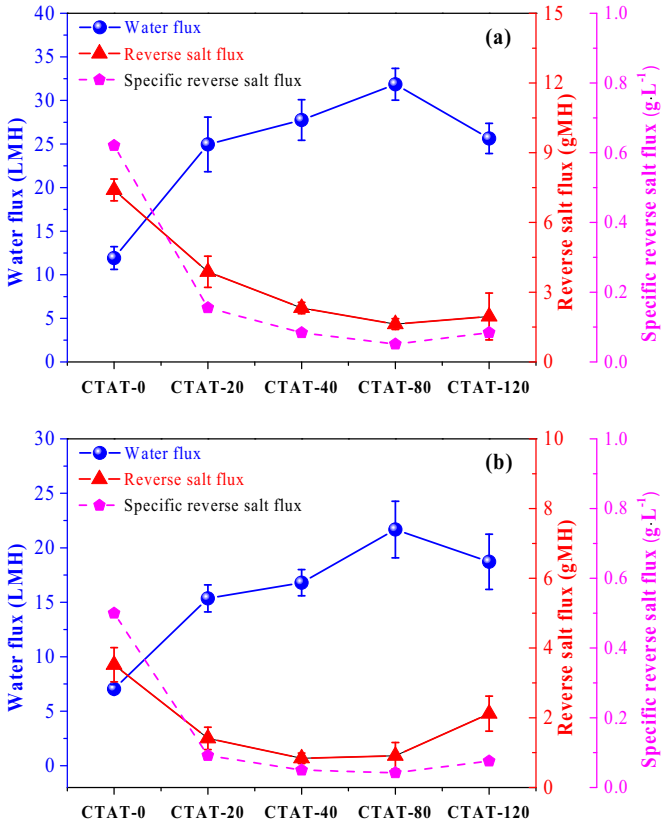

Fig. 6. FO performance of the TFC FO membrane in PRO and FO modes.

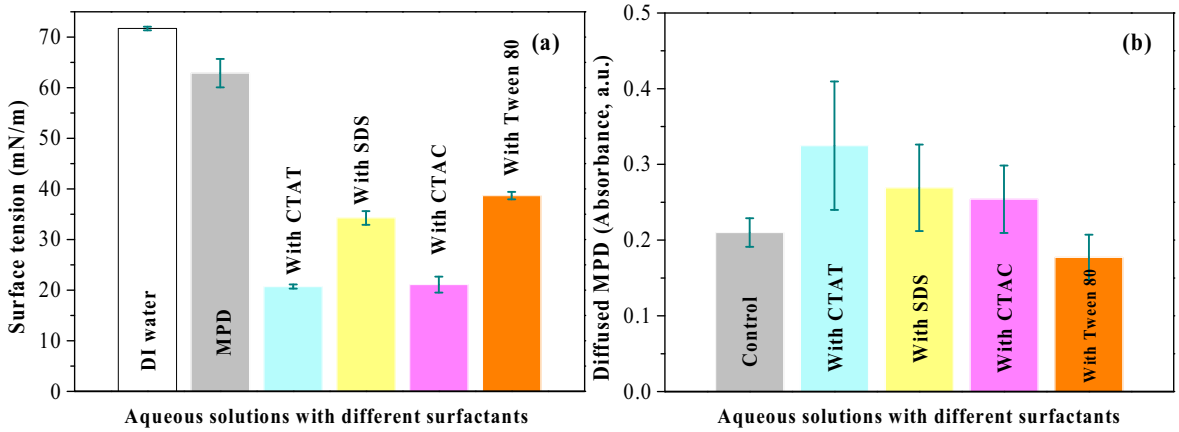

Fig. 7. Effect of surfactant types on the (a) surface tension and (b) MPD diffusion behavior of corresponding MPD and MPD/surfactant aqueous solutions. It is noted that the concentration of surfactants incorporated in MPD solutions was all controlled at 80 mg·L^{-1}.

therefore the improvement of membrane permeability.

3.3. Separation performance evaluation of TFC membrane

The intrinsic separation properties of the fabricated TFC membranes were measured and the results are summarized in Table 2. With the increase of the CTAT content, the selectivity of resulted TFC membranes shows the increasing tendency as indicated by the higher rejection of NaCl, because of the higher crosslinking degree of PA layer as discussed before. It also can be found that the modified TFC membranes exhibit the overall higher water permeability coefficient and rejection of NaCl, demonstrating the beneficial impact of incorporating CTAT in the amino monomer. For the modified TFC membrane, the water permeability coefficient increases from 1.59 ± 0.24 L·m^{-2}·h^{-1}·bar^{-1} of CTAT-20 membrane to 3.11 ± 0.14 L·m^{-2}·h^{-1}·bar^{-1} of CTAT-80 membrane which is roughly consistence with the variation trend of the improved membrane hydrophilicity (Fig. 5) and the rougher membrane surface (Fig. 4). Also, the thickness of the PA layer decreases from 230.1 ± 29.7 nm of CTAT-20 to 190.1 ± 10.9 nm of CTAT-80 as marked in Fig. S4, which facilitates the transport of water molecules across the membrane to some extent as a result of the reduced permeation resistance. However, CTAT-120 membrane exhibits the diminished water permeability coefficient and the slightly lower salt rejection, mainly due to the thicker PA layer with a relatively lower crosslinking degree as demonstrated before. The salt permeation coefficient presents the similar trend with that of the water permeability. In addition, the variation trend of the B/A ratio of the fabricated TFC membranes is roughly on the contrary with that of the NaCl rejection performance derived from the improved membrane selectivity.

Accordingly, FO performance tests of TFC membranes was performed and the results are shown in Fig. 6. Generally, the water fluxes and reverse salt fluxes of the pristine and modified TFC membranes in both FO and PRO modes are highly consistent with those variation trend of their intrinsic separation properties. TFC membranes with the increase of CTAT content in amino solution exhibit the higher water flux and reduced reverse salt flux. In addition to the evidently improved water fluxes (J_V) of 31.8 and 21.7 LMH, CTAT-80 membranes correspondingly achieve the specific reverse salt fluxes of 0.06 and 0.04 g L^{-1} in PRO and FO modes respectively. Therefore, it can be concluded that the CTAT-80 membrane shows the excellent separation performance compared with others, and the addition of CATA at the concentration of 80 mg L^{-1} is preferred for the optimized preparation condition for the further comparative study.

3.4. Comparative study on TFC membranes with different surfactants

To elaborate the beneficial impact brought by the incorporation of CTAT during IP and further unravel the modification mechanism, the comparative study was also performed by using CTAC as additive since it comprises the same alkane group as the hydrophobic tail but different hydrophilic head as shown in Fig. S1, in comparison with those of the CTAT. Meanwhile, the ionic and nonionic surfactants of SDS and Tween

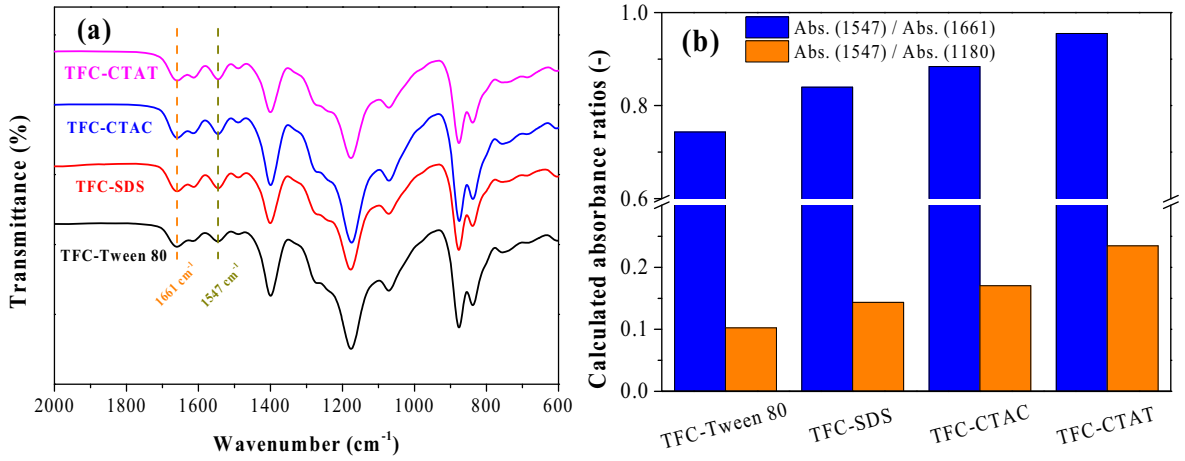

Fig. 8. (a) ATR-FTIR spectra of the TFC membranes with different surfactants incorporated in MPD solution and (b) the corresponding absorbance ratios of Abs. (-CONH-) / Abs. (-COOH) and Abs. (-CONH-) / Abs. (C—F).

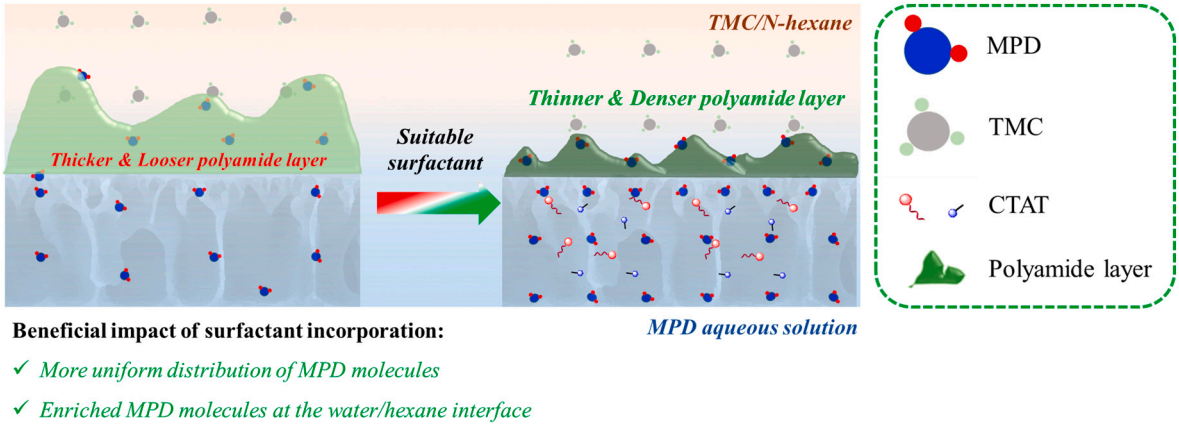

Fig. 9. Schematic of the beneficial impact of surfactant incorporation on the formation of resultant PA layer.

80 were also included.

Because the addition of surfactant effectively reduces the surface tension of aqueous solutions and therefore facilitates the transport of amino monomers towards to the organic phase to some extent, the change of the surface tensions for MPD solutions incorporated with different surfactants was measured and the results are shown in Fig. 7 (a). For comparison, the surface tensions of DI water and the pure MPD aqueous solution are also included. It can be seen that the surface tension of DI water is 71.7 mN/m, in accordance with the results as reported by others [41]. While the decreased surface tension for the pure MPD aqueous solution illustrates the surface-active characteristics of MPD. After adding different surfactants, the surface tensions of corresponding solutions overall decrease which follows the sequence of MPD > Tween 80-MPD > SDS-MPD > CTAC-MPD > CTAT-MPD, and the MPD solution containing CTAT surfactant exhibits the lowest surface tension of 20.7 mN/m. The decreased surface tension would be beneficial for the reaction between MPD and TMC [38,45,60], and therefore favors the rougher and denser formation of PA layer as discussed before. Meanwhile, the incorporation of CTAT at the given experimental condition exhibits the most significant impact on the enhancement of MPD diffusion behavior in comparison with those other surfactants.

Similarly, the chemical properties of fabricated TFC membrane with different surfactants incorporated in MPD solutions were characterized by ATR-FTIR. As shown in Fig. 8 (a), characteristic peaks of PA can be found in the spectra of all the fabricated TFC membrane. The absorbance ratio of Abs. (1547) / Abs. (1661) and Abs. (1547) / Abs. (1180) was calculated and the results are presented in Fig. 8 (b). The original data are summarized in Tables S5 and S6 of the **Supporting Information**. Overall, the two absorbance ratios of the modified membranes are higher than those of the pristine TFC membrane (Fig. 2 (b)), attributed to the reduced surface tensions of amino aqueous solution with surfactants as discussed before. Furthermore, it also can be found that the change of these two absorbance ratios of modified membranes follows the sequence of TFC-Tween 80 < TFC-SDS < TFC-CTAC < TFC-CTAT, which is highly in consistent with the change of the surface tension of solutions incorporated with different surfactants. These results demonstrate again that the reduced surface tension is considered as the prerequisite for accelerating the interfacial polymerization process as reported elsewhere [31,38,41]. In addition, results in Fig. S5 in the **Supporting Information** also demonstrate that the variation trend of d-spacing of modified membranes follows the sequence of TFC-Tween 80 > TFC-SDS > TFC-CTAC > TFC-CTAT under the given preparation conditions, which is roughly in accordance with those of their cross-linking degree as discussed before.

Since the IP reaction between MPD and TMC is a reaction-diffusion process far from thermodynamic equilibrium [31]. As a result of the combined factors of the reduced surface tension and the interaction between MPD monomers and surfactants, the stocking and distribution of MPD monomer and the diversity of the diffusion rate of MPD from the aqueous phase to the organic phase might dominantly determine the IP

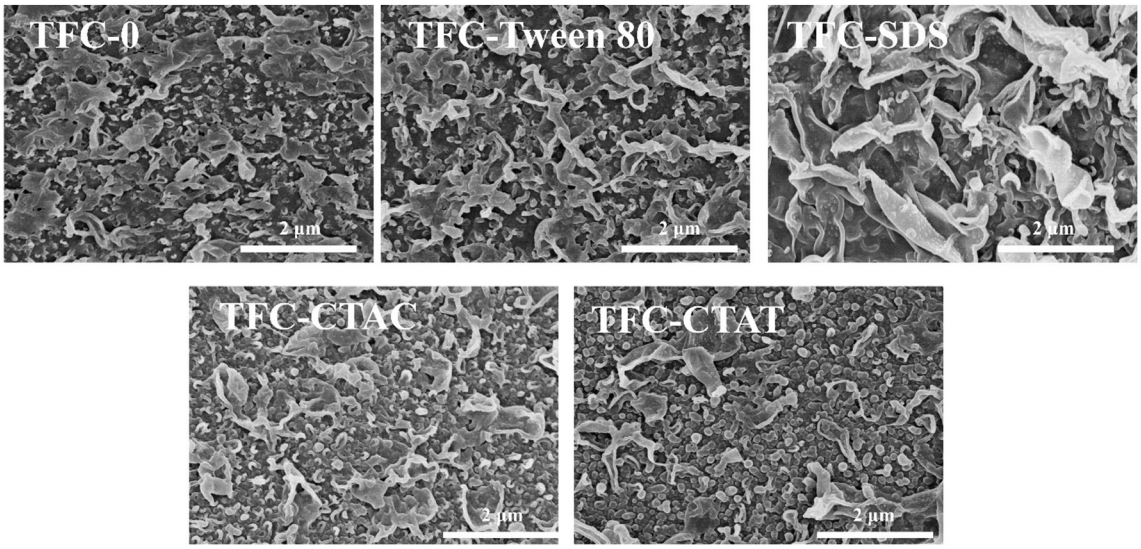

Fig. 10. Top surface morphology of the pristine and modified TFC membranes. The scale bar in the picture represents the length of 2.0 μm.

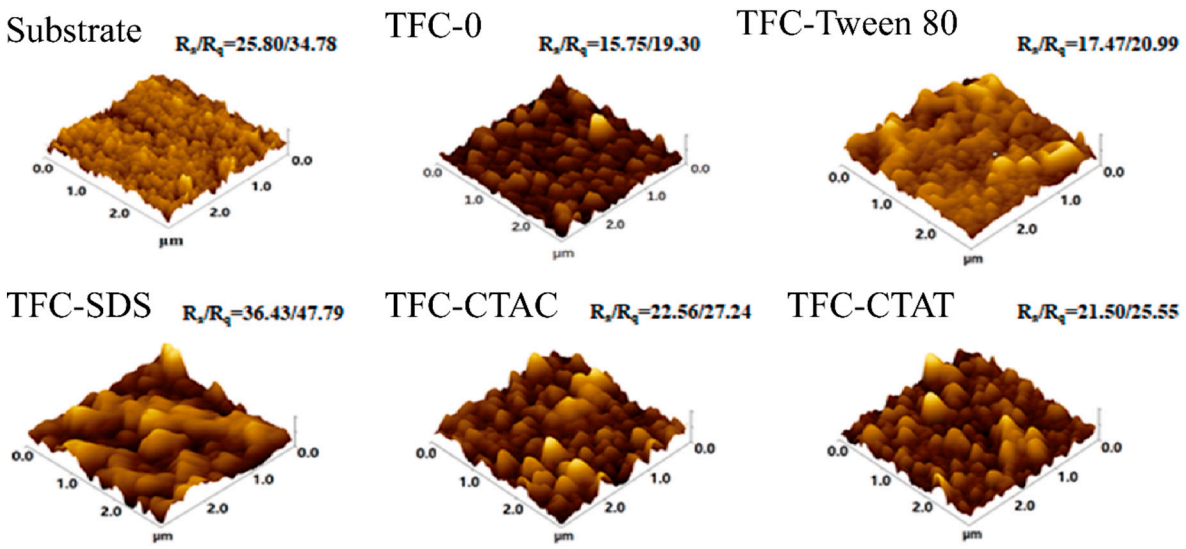

Fig. 11. AFM images of the substrate, pristine and modified TFC membranes with different surfactants.

reaction. In addition to the unremarkable impact on reducing the surface tension of MPD solution, the incorporation of Tween 80 also attenuates the MPD diffusion towards the organic phase. Therefore, it is assumed that the incorporation of Tween 80 might result in the formation of the thick PA layer with relative low crosslinking degree in comparison with those of CTAT, on the basis of the formation mechanism as discussed before. In addition, on the basis of the investigation by Jia et al. [40], the ionic interaction between MPD and the positively charged quaternary ammonium head in CTAC could regulate the uniform distribution of MPD molecules around CTAC surfactants and maintain the amine group of MPD away from CTAC. Therefore, it can be concluded that the enriched MPD molecules with uniform distribution at the water/hexane interface is beneficial for the formation of a nascent PA layer with high crosslinking degree in the initial stage of IP. Subsequently, the adequate crosslinking reaction is resulted by the significantly reduced surface tensions for the TFC-CTAC and TFC-CTAT membranes (Fig. 7 (a)). Such beneficial effect reasonably leads to the resultant PA layer with the higher crosslinking degree and less defects [61,62]. Besides, in comparison with the component of chloride ions (Cl^-) in CTAC, the toluene-p-sulphonate component in CTAT also exhibits the enhanced interaction with MPD through the π-π conjunction of the benzene ring structure and the electrostatic interaction between negatively charged sulfonated groups and the hydrolyzed -NH_2H^+ group in MPD. It might disorder the molecular chains of PA and favors the higher crosslinking degree since the regular formation of PA shows highly crystalline molecular segments in the polymer but low crosslinking degree [31]. Moreover, the existence of the toluene-p-sulphonate component in CTAT also imposes the larger steric hindrance which constrains the diffusion of PA fragments to water and therefore the unexpected hydrolysis of the PA [38], and thereby leads to the higher crosslinking degree of TFC-CTAT in comparison with that of TFC-CTAC. Fig. 9 depicts the benefits of the suitable surfactant (herein CTAT) incorporated in amine solution and its positive impacts on the formation of resultant PA layer with the reduced thickness and the higher crosslinking degree. For TFC-SDS membrane with the presence of ionic surfactant in amine solution, the intensified Marangoni convection promotes the MPD diffusion and reshapes the nascent PA layer, and consequently generates a thicker, rougher and stacked PA layer as widely reported elsewhere [41,63,64]. The proposed mechanism would be further verified by the characterizations and performance tests as follows.

It can be found from Fig. 10 that, in comparison with the pristine TFC membrane, the modified TFC membranes show the uniform and defect-free PA layer by taking advantage of the higher loading amount of MPD

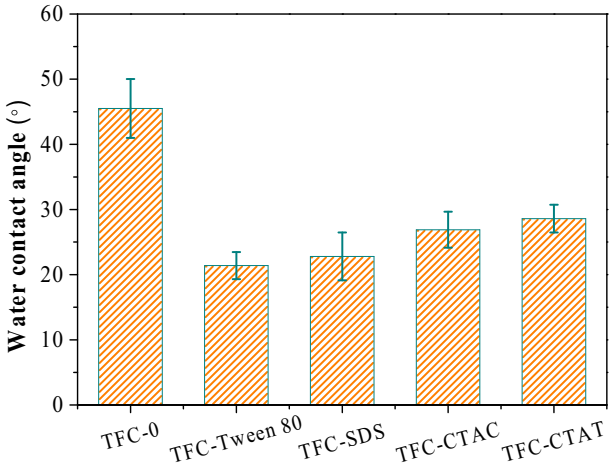

Fig. 12. WCA of the pristine and the modified TFC membranes.

on membrane substate, resulted from the reduced surface tension of amine solutions with surfactants as aforementioned. While for TFC-CTAC and TFC-CTAT membranes with almost the equal surface tension of the amine solutions (Fig. 7 (a)), the more intensive interaction between CTAT and MPD might effectively achieve the accumulation and dispersion of MPD a the interface between the aqueous and organic phase, and therefore results in the formation of the nascent PA layer with the relatively high crosslinking degree. Besides, the migration of MPD molecules could hardly breakthrough the nascent PA layer and results in the more obvious nodule-like structure. For the surface features of TFC-SDS membrane, the formation of the larger dimensional leaf-like structure (also called the clumpy roof-like structure) could also be interpreted by the proposed modification mechanism, since SDS leads to the moderate decrease of surface tension and therefore the formation of a relatively loose PA nascent layer. Besides, the accelerated MPD diffusion behavior promotes the reshape process of the nascent PA layer and consequently leads to the crumply rough surface with big leaf-like structure. Besides, the difference in the surface roughness of as-fabricated TFC membranes was also characterized by AFM characterization and the images are delineated in Fig. 11. In comparison with the substrate membrane, the relatively smoother surface of TFC-0 originates from the immobilization of PA layer which fills the ravine on PVDF

Table 3
Intrinsic separation properties of the pristine and modified TFC membrane with different surfactants incorporated.

Membrane No.	Rejection of NaCl(%)	A (L m^{-2} h^{-1} bar^{-1})	B (L m^{-2} h^{-1})	B/A (bar)
TFC-0	85.59 ± 4.00	0.71 ± 0.08	0.49 ± 0.01	0.69 ± 0.01
TFC-Tween 80	90.10 ± 2.00	2.49 ± 0.23	1.21 ± 0.18	0.48 ± 0.07
TFC-SDS	94.90 ± 1.40	2.13 ± 0.15	1.38 ± 0.14	0.66 ± 0.06
TFC-CTAC	95.15 ± 2.27	2.96 ± 0.65	0.94 ± 0.05	0.31 ± 0.02
TFC-CTAT	96.01 ± 1.67	3.11 ± 0.14	0.93 ± 0.14	0.30 ± 0.04

substrate. The modified TFC membranes shows the relatively smoother surface and the values of the averaged surface roughness locate in the region between 17 and 22 nm, except for TFC-SDS membrane with the much rougher surface, as indicated by the abrupt higher surface roughness of 36.4 nm. Accordingly, above results of ATR-FTIR, SEM and AFM could be reasonably interpreted by the modification mechanism as proposed.

Fig. 12 depicts the WCA results of the pristine and modified TFC membranes. Generally, the pristine TFC membrane exhibits a WCA of 45.5 ± 4.5° which is much higher than those of the modified membranes, indicating its relatively poorer hydrophilicity. Besides, there is no obvious difference between the WCAs of the modified TFC membranes. It is widely acknowledged that the combined factors of the chemical property and roughness of the membrane surface affects the surface wettability. The lowest WCAs of TFC-Tween 80 might be ascribed to the less crosslinked PA layer and the accordingly the larger proportion of hydrophilic carboxyl groups resulted from the hydrolysis of un-reacted acyl chloride groups in TMC monomer. In addition to the similar surface roughness, the highly crosslinked PA layer for TFC-CTAT and TFC-CTAT membranes might be the possible reason for the overall higher WCA.

The results of the intrinsic separation properties of the pristine and modified TFC membranes are summarized in Table 3. It can be found that the water permeability coefficient of four modified membranes (2.49 ± 0.23, 2.13 ± 0.15, 2.96 ± 0.65 and 3.11 ± 0.14) are all evidently higher than the pristine membrane (0.71 ± 0.08), which possibly ascribed to the lower permeation resistance and the higher permeation area resulted from the reduced thickness of PA layer (Fig. S6) and the rougher PA morphology (Fig. 11). Moreover, the variation of the NaCl rejection performance is roughly accordance with the calculated crosslinking degree based from the ATR-FTIR spectra of the fabricated TFC membranes, since the higher crosslinking degree of the fabricated TFC membrane exhibits the higher rejection rate of NaCl. The accordant results of salt permeability coefficient and the parameters of B/A are also accordingly observed, which are overall contrary to that of the solute rejection performance of correspondingly membranes. Based from above results, the incorporation of CTAT in amine solution not only improves the water permeance, but also promote the selectivity of the resultant TFC membrane (TFC-CTAT), which potentially shows the elevated operation efficiency as well as the improved selectivity in FO process compared with the others.

Additionally, the FO performance tests of fabricated TFC membrane in both FO and PRO modes were performed in order to evaluate the

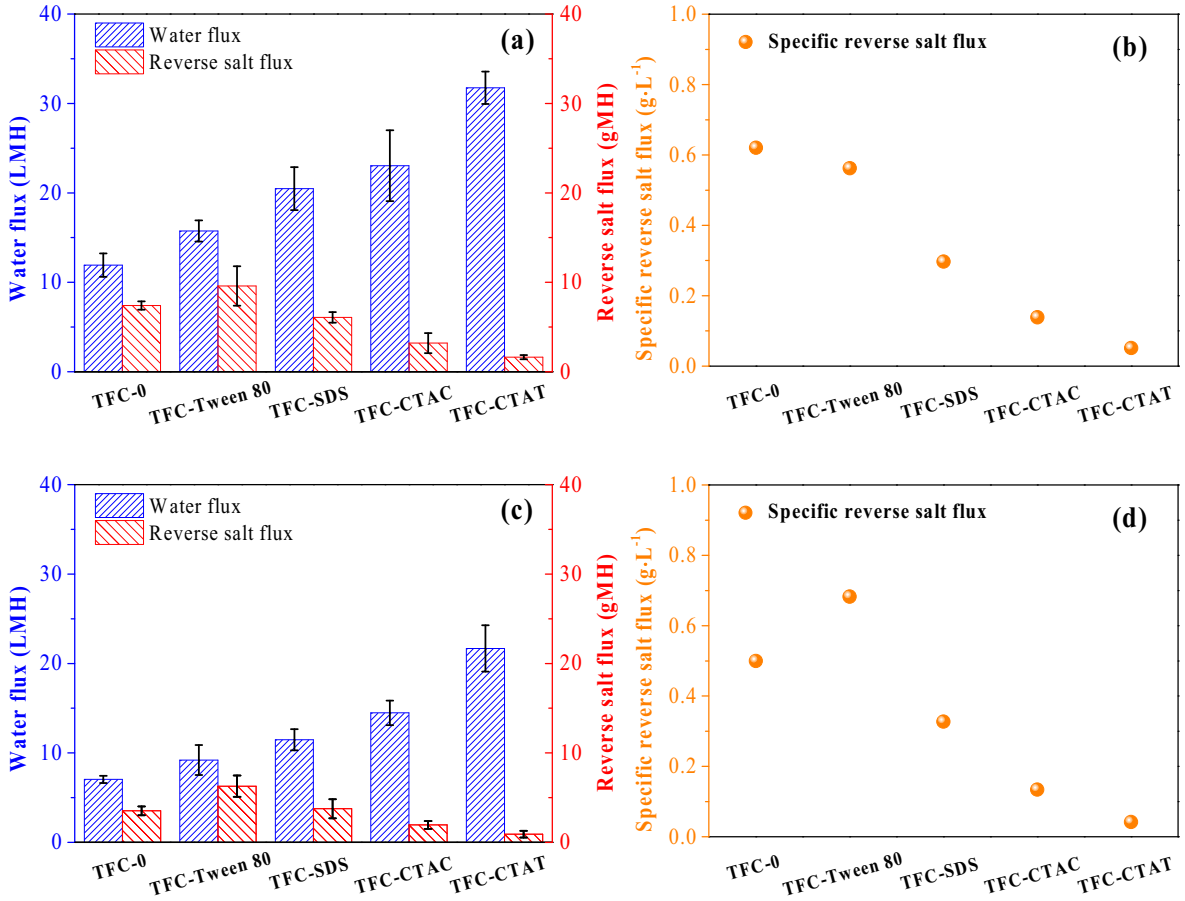

Fig. 13. FO performance and the calculated values of the specific reverse salt of the pristine and modified TFC membrane in PRO (a and b) and FO (c and d) modes.

Table 4
FO performance benchmarking of the fabricated TFC-CTAT membrane in the current study compared to those membranes reported by prior pioneering investigations.

Membranes	J_V (LMH)	J_S (gMH)	J_S/J_V (g·L^{-1})	Feed/ Draw solutions	Mode	Reference
MPD + CTAT/ TMC	31.8	1.6	0.05	DI water/ 1 M NaCl	PRO	This work
MPD + CTAT/ TMC	21.7	0.9	0.04	DI water/ 1 M NaCl	FO	This work
MPD + GO/ TMC	24.7	5.2	0.21	DI water/ 0.5 M NaCl	FO	[65]
MPD + HMTA/ TMC	50.6	7.5	0.15	DI water/ 2 M NaCl	PRO	[12]
MPD + GO/ TMC	30	7.5	0.25	DI water/ 1 M NaCl	PRO	[33]
MPD + S-GO/TMC	29.9	3.9	0.13	DI water/ 1 M NaCl	FO	[66]
MPD/TMC + NH_2-UiO-66	29.7	4.7	0.16	DI water/ 1 M NaCl	FO	[67]
MPD/TMC + UiO-66	36.7	7.1	0.19	DI water/ 1 M NaCl	PRO	[68]
MPD + DA/ TMC	50.5	8.2	0.16	DI water/ 1 M NaCl	FO	[69]
MPD + SDS/ TMC	45.1	~22.1	0.49	DI water/ 1 M NaCl	PRO	[70]

enhanced perm-selectivity of TFC membrane with the surfactants incorporated. It can be found in Fig. 13 that the water flux of TFC membranes is substantially in consistence with their water permeability coefficient as listed in Table 3 except for TFC-Tween 80. Additionally, the reverse salt flux of the fabricated TFC membranes is overall in keeping with those of their rejection performance towards NaCl. Amongst these modified membranes with different surfactants incorporated, TFC-CTAT is capable of the highest water flux as well as the best selectivity, as indicated by the lowest specific reverse salt fluxes of 0.06 and 0.04 g·L^{-1} in PRO and FO modes respectively.

3.5. Performance benchmarking

Table 4 summarizes the parameters of water flux, reverse salt flux and correspondingly the specific reverse salt flux of reported TFC membranes as a comparison with TFC-CTAT membranes. In comparison with those TFC-FO membrane with the in-situ modification of the PA layer, the TFC-CTAT membrane in this study achieves a comparable water flux accompanied with a much lower value of the specific reverse salt flux, indicating the obviously improved selectivity. Such improvement suggests that the perm-selectivity of TFC membranes could be effectively promoted by taking advantage of the beneficial effects brought by suitable surfactants.

4. Conclusions

In this work, the surfactant-induced intervention in interfacial polymerization was performed for by incorporating hexadecyltrimethylammonium toluene-p-sulphonate (CTAT) into the amine aqueous solution for developing the highly-permeable TFC membrane with exceptional selectivity. The effect of CTAT content on the physicochemical properties of PA layer and therefore the FO performance was systemically investigated by conventional characterizations and a series of performance tests. To further elaborate the underlying mechanism of performance improvement, three typical surfactants at the optimized concentration were also employed and studied for comparison. The results indicate the existence of toluene-p-sulphonate component in CTAT should be responsible for the improved perm-selectivity of resultant TFC membrane by taking advantage of the uniform distribution and accumulation of amine monomer at the interface between water and organic phase and the promoted interfacial polymerization reaction, as a result of the reduced surface tension. Consequently, the TFC-CTAT membrane prepared at the optimal condition exhibits the improved fluxes of 31.8 and 21.7 LMH, accompanied with the low specific reverse salt flux of 0.05 and 0.04 g·L^{-1} in PRO and FO testing modes, using 1 M NaCl aqueous solution and DI water as the draw and feed solutions. The membrane performance is comparable with those pioneering works published in recent years. Therefore, this work offers a simple but promising strategy for developing TFC-FO membrane with high permeability and selectivity.

CRediT authorship contribution statement

Xuan Zhang: Conceptualization, Investigation, Data curation, Writing – original draft, Writing – review & editing. **Hui-Min Cui:** Conceptualization, Investigation, Data curation. **Yu Gao:** Investigation. **Zhi-Wei Yan:** Investigation. **Xi Yan:** Investigation, Validation. **Yan Chen:** Investigation, Methodology. **Xiao-Jing Guo:** Investigation, Methodology. **Wan-Zhong Lang:** Conceptualization, Supervision, Methodology, Writing – review & editing.

Declaration of competing interest

The authors declare that they have no known competing financial interests or personal relationships that could have appeared to influence the work reported in this paper.

Data availability

Data will be made available on request.

Acknowledgments

The research is supported by National Natural Science Foundation of China (22278267; 22005191), “111” Innovation and Talent Recruitment Base on Photochemical and Energy Materials (No. D18020), Shanghai Engineering Research Center of Green Energy Chemical Engineering (No. 18DZ2254200). The authors also would like to thank the engineers from Shiyanjia Lab (www.shiyanjia.com) for their kind help with XPS characterization.

Appendix A. Supplementary data

Supplementary data to this article can be found online at https://doi.org/10.1016/j.desal.2023.116617.

References

[1] X. Yi, H. Zhong, M. Xie, P. Zhao, W. Song, X. Wang, Novel insights on fouling mechanism of forward osmosis membrane during deep thickening waste activated sludge, J. Membr. Sci. 660 (2022), 120894, https://doi.org/10.1016/j.memsci.2022.120894.
[2] J. Wang, X. Liu, Forward osmosis technology for water treatment: recent advances and future perspectives, J. Clean. Prod. 280 (2021), 124354, https://doi.org/10.1016/j.jclepro.2020.124354.
[3] N.D. Suzaimi, P.S. Goh, A.F. Ismail, S.C. Mamah, N. Malek, J.W. Lim, K.C. Wong, N. Hilal, Strategies in forward osmosis membrane substrate fabrication and modification: a review, Membranes (Basel) 10 (11) (2020) 332–374, https://doi.org/10.3390/membranes10110332.
[4] Q. Wang, Z. Zhou, J. Li, Q. Tang, Y. Hu, Modeling and measurement of temperature and draw solution concentration induced water flux increment efficiencies in the forward osmosis membrane process, Desalination 452 (2019) 75–86, https://doi.org/10.1016/j.desal.2018.11.001.
[5] J. Zhang, D. Wang, Y. Chen, B. Gao, Z. Wang, Scaling control of forward osmosis-membrane distillation (FO-MD) integrated process for pre-treated landfill leachate

treatment, Desalination 520 (2021), 115342, https://doi.org/10.1016/j.desal.2021.115342.
[6] A. Tiraferri, N.Y. Yip, A.P. Straub, S. Romero-Vargas Castrillon, M. Elimelech, A method for the simultaneous determination of transport and structural parameters of forward osmosis membranes, J. Membr. Sci. 444 (2013) 523–538, https://doi.org/10.1016/j.memsci.2013.05.023.
[7] T.Y. Cath, A.E. Childress, M. Elimelech, Forward osmosis: principles, applications, and recent developments, J. Membr. Sci. 281 (1) (2006) 70–87, https://doi.org/10.1016/j.memsci.2006.05.048.
[8] X. Chen, J. Xu, J. Lu, B. Shan, C. Gao, Enhanced performance of cellulose triacetate membranes using binary mixed additives for forward osmosis desalination, Desalination 405 (2017) 68–75, https://doi.org/10.1016/j.desal.2016.12.003.
[9] K. Zhang, X. An, Y. Bai, C. Shen, Y. Jiang, Y. Hu, Exploration of food preservatives as draw solutes in the forward osmosis process for juice concentration, J. Membr. Sci. 635 (2021), 119495, https://doi.org/10.1016/j.memsci.2021.119495.
[10] H.-Q. Liang, W.-S. Hung, H.-H. Yu, C.-C. Hu, K.-R. Lee, J.-Y. Lai, Z.-K. Xu, Forward osmosis membranes with unprecedented water flux, J. Membr. Sci. 529 (2017) 47–54, https://doi.org/10.1016/j.memsci.2017.01.056.
[11] K. Lutchmiah, A.R. Verliefde, K. Roest, L.C. Rietveld, E.R. Cornelissen, Forward osmosis for application in wastewater treatment: a review, Water Res. 58 (2014) 179–197, https://doi.org/10.1016/j.watres.2014.03.045.
[12] L. Shen, L. Tian, J. Zuo, X. Zhang, S. Sun, Y. Wang, Developing high-performance thin-film composite forward osmosis membranes by various tertiary amine catalysts for desalination, Adv. Compos. Hybrid. Mater. 2 (1) (2018) 51–69, https://doi.org/10.1007/s42114-018-0070-1.
[13] L. Shen, J. Zuo, Y. Wang, Tris(2-aminoethyl)amine in-situ modified thin-film composite membranes for forward osmosis applications, J. Membr. Sci. 537 (2017) 186–201, https://doi.org/10.1016/j.memsci.2017.05.035.
[14] X. Song, L. Wang, C.Y. Tang, Z. Wang, C. Gao, Fabrication of carbon nanotubes incorporated double-skinned thin film nanocomposite membranes for enhanced separation performance and antifouling capability in forward osmosis process, Desalination 369 (2015) 1–9, https://doi.org/10.1016/j.desal.2015.04.020.
[15] F. Yu, H. Shi, J. Shi, K. Teng, Z. Xu, X. Qian, High-performance forward osmosis membrane with ultra-fast water transport channel and ultra-thin polyamide layer, J. Membr. Sci. 616 (2020), 118611, https://doi.org/10.1016/j.memsci.2020.118611.
[16] M. Kahrizi, R.R. Gonzales, L. Kong, H. Matsuyama, P. Lu, J. Lin, S. Zhao, Significant roles of substrate properties in forward osmosis membrane performance: a review, Desalination 528 (2022), 115615, https://doi.org/10.1016/j.desal.2022.115615.
[17] X. Zhang, L. Shen, W.-Z. Lang, Y. Wang, Improved performance of thin-film composite membrane with PVDF/PFSA substrate for forward osmosis process, J. Membr. Sci. 535 (2017) 188–199, https://doi.org/10.1016/j.memsci.2017.04.038.
[18] Y. Zhao, G.S. Lai, J.Y. Chong, R. Wang, Dissecting the structure-compaction-performance relationship of thin-film composite polyamide membranes with different structure features, J. Membr. Sci. 654 (2022), 120553, https://doi.org/10.1016/j.memsci.2022.120553.
[19] J. Farahbakhsh, V. Vatanpour, M. Khoshnam, M. Zargar, Recent advancements in the application of new monomers and membrane modification techniques for the fabrication of thin film composite membranes: a review, React. Funct. Polym. 166 (2021), 105015, https://doi.org/10.1016/j.reactfunctpolym.2021.105015.
[20] L. Xu, T. Yang, M. Li, J. Chang, J. Xu, Thin-film nanocomposite membrane doped with carboxylated covalent organic frameworks for efficient forward osmosis desalination, J. Membr. Sci. 610 (2020), 118111, https://doi.org/10.1016/j.memsci.2020.118111.
[21] N. Sun, P. Dou, W. Zhai, H. He, L.D. Nghiem, V. Vatanpour, Y. Zhang, C. Liu, T. He, Polyethylene separator supported thin-film composite forward osmosis membranes for concentrating lithium enriched brine, Water Res. 216 (2022), 118297, https://doi.org/10.1016/j.watres.2022.118297.
[22] C. Ji, Z. Zhai, C. Jiang, P. Hu, S. Zhao, S. Xue, Z. Yang, T. He, Q.J. Niu, Recent advances in high-performance TFC membranes: a review of the functional interlayers, Desalination 500 (2021), 114869, https://doi.org/10.1016/j.desal.2020.114869.
[23] Y. Tang, H. Yu, Y. Xing, C. Gao, J. Xu, Microstructure and desalination performance of polyamide membranes interfacially regulated via single-side post-modified CNTs networks, Desalination 482 (2020), 114408, https://doi.org/10.1016/j.desal.2020.114408.
[24] D. Wang, J. Li, B. Gao, Y. Chen, Z. Wang, Triple-layered thin film nanocomposite membrane toward enhanced forward osmosis performance, J. Membr. Sci. 620 (2021), 118879, https://doi.org/10.1016/j.memsci.2020.118879.
[25] C. Tang, Z. Wang, I. Petrinić, A.G. Fane, C. Hélix-Nielsen, Biomimetic aquaporin membranes coming of age, Desalination 368 (2015) 89–105, https://doi.org/10.1016/j.desal.2015.04.026.
[26] M. Xie, W. Luo, H. Guo, L.D. Nghiem, C.Y. Tang, S.R. Gray, Trace organic contaminant rejection by aquaporin forward osmosis membrane: transport mechanisms and membrane stability, Water Res. 132 (2018) 90–98, https://doi.org/10.1016/j.watres.2017.12.072.
[27] W. Ghamri, P. Loulergue, I. Petrinić, C. Hélix-Nielsen, M. Pontié, N. Nasrallah, K. Daoud, A. Szymczyk, Impact of sodium hypochlorite on rejection of non-steroidal anti-inflammatory drugs by biomimetic forward osmosis membranes, J. Membr. Sci. 633 (2021), 119388, https://doi.org/10.1016/j.memsci.2021.119388.
[28] L. Xia, M.F. Andersen, C. Hélix-Nielsen, J.R. McCutcheon, Novel commercial aquaporin flat-sheet membrane for forward osmosis, Ind. Eng. Chem. Res. 56 (41) (2017) 11919–11925, https://doi.org/10.1021/acs.iecr.7b02368.
[29] L. Zhao, Z. Liu, F. Soyekwo, C. Liu, Y. Hu, Q.J. Niu, Exploring the feasibility of novel double-skinned forward osmosis membranes with higher flux and superior anti-fouling properties for sludge thickening, Desalination 523 (2022), 115410, https://doi.org/10.1016/j.desal.2021.115410.
[30] J.R. Werber, A. Deshmukh, M. Elimelech, The critical need for increased selectivity, not increased water permeability, for desalination membranes, Environ. Sci. Technol. Lett. 3 (4) (2016) 112–120, https://doi.org/10.1021/acs.estlett.6b00050.
[31] Q. Jia, Y. Li, L. Zhong, Y. Liu, D. Duan, The role of phase transfer catalysts on properties of polyamide thin-film composite forward osmosis membranes, Chem. Eng. J. 426 (2021), 128989, https://doi.org/10.1016/j.cej.2021.128989.
[32] J. Li, L. Cheng, W. Song, Y. Xu, F. Liu, Z. Wang, In-situ sol-gel generation of SiO2 nanoparticles inside polyamide membrane for enhanced nanofiltration, Desalination 540 (2022), 115981, https://doi.org/10.1016/j.desal.2022.115981.
[33] L. Shen, S. Xiong, Y. Wang, Graphene oxide incorporated thin-film composite membranes for forward osmosis applications, Chem. Eng. Sci. 143 (2016) 194–205, https://doi.org/10.1016/j.ces.2015.12.029.
[34] Z. Tan, S. Chen, X. Peng, L. Zhang, C. Gao, Polyamide membranes with nanoscale turing structures for water purification, Science 360 (6388) (2018) 518–521, https://doi.org/10.1126/science.aar6308.
[35] T. Kamada, T. Ohara, T. Shintani, T. Tsuru, Optimizing the preparation of multi-layered polyamide membrane via the addition of a co-solvent, J. Membr. Sci. 453 (2014) 489–497, https://doi.org/10.1016/j.memsci.2013.11.028.
[36] Q. Gan, L.E. Peng, H. Guo, Z. Yang, C.Y. Tang, Cosolvent-assisted interfacial polymerization toward regulating the morphology and performance of polyamide reverse osmosis membranes: increased m-phenylenediamine solubility or enhanced interfacial vaporization? Environ. Sci. Technol. 56 (14) (2022) 10308–10316, https://doi.org/10.1021/acs.est.2c01140.
[37] M.B.M.Y. Ang, Y.-T. Lu, S.-H. Huang, J.C. Millare, H.-A. Tsai, K.-R. Lee, Surfactant-assisted interfacial polymerization for improving the performance of nanofiltration-like forward osmosis membranes, J. Polym. Res. 29 (3) (2022) 90–99, https://doi.org/10.1007/s10965-022-02942-6.
[38] Y. Liang, Y. Zhu, C. Liu, K.R. Lee, W.S. Hung, Z. Wang, Y. Li, M. Elimelech, J. Jin, S. Lin, Polyamide nanofiltration membrane with highly uniform sub-nanometre pores for sub-1 a precision separation, Nat. Commun. 11 (1) (2020) 2015–2024, https://doi.org/10.1038/s41467-020-15771-2.
[39] Y. Mansourpanah, S.S. Madaeni, A. Rahimpour, Fabrication and development of interfacial polymerized thin-film composite nanofiltration membrane using different surfactants in organic phase; study of morphology and performance, J. Membr. Sci. 343 (1–2) (2009) 219–228, https://doi.org/10.1016/j.memsci.2009.07.033.
[40] Q. Jia, H. Han, L. Wang, B. Liu, H. Yang, J. Shen, Effects of CTAC micelles on the molecular structures and separation performance of thin-film composite (TFC) membranes in forward osmosis processes, Desalination 340 (2014) 30–41, https://doi.org/10.1016/j.desal.2014.02.017.
[41] S.-J. Park, M.-S. Lee, W. Choi, J.-H. Lee, Biocidal surfactant-assisted fabrication of thin film composite membranes with excellent and durable anti-biofouling performance, Chem. Eng. J. 431 (2022), 134114, https://doi.org/10.1016/j.cej.2021.134114.
[42] Q. Gan, L.E. Peng, Z. Yang, P.-F. Sun, L. Wang, H. Guo, C.Y. Tang, Demystifying the role of surfactant in tailoring polyamide morphology for enhanced reverse osmosis performance: mechanistic insights and environmental implications, Environ. Sci. Technol. 57 (4) (2023) 1819–1827, https://doi.org/10.1021/acs.est.2c08076.
[43] M.B.M.Y. Ang, C.-L. Tang, M.R. De Guzman, H.L.C. Maganto, A.R. Caparanga, S.-H. Huang, H.-A. Tsai, C.-C. Hu, K.-R. Lee, J.-Y. Lai, Improved performance of thin-film nanofiltration membranes fabricated with the intervention of surfactants having different structures for water treatment, Desalination 481 (2020), 114352, https://doi.org/10.1016/j.desal.2020.114352.
[44] X. Zhang, S. Xiong, C.-X. Liu, L. Shen, C. Ding, C.-Y. Guan, Y. Wang, Confining migration of amine monomer during interfacial polymerization for constructing thin-film composite forward osmosis membrane with low fouling propensity, Chem. Eng. Sci. 207 (2019) 54–68, https://doi.org/10.1016/j.ces.2019.06.010.
[45] Y. Li, T.-H. Chen, C.-Y. Yu, T. Wu, X.-T. Zhao, J.-F. Pan, L.-F. Liu, Facile polyamide microstructure adjustment of the composite reverse osmosis membrane assisted by PF127/SDS mixed micelles for improving seawater desalination performance, Desalination 521 (2022), 115395, https://doi.org/10.1016/j.desal.2021.115395.
[46] H.-M. Cui, X. Yan, Y. Chen, W.-Y. Xu, W.-Z. Lang, Enhanced performance of forward osmosis membranes by incorporating PVDF substrates with hydrophilic nanofillers, Desalin. Water Treat. 155 (2019) 1–14.
[47] Y. Wang, R. Ou, Q. Ge, H. Wang, T. Xu, Preparation of polyethersulfone/carbon nanotube substrate for high-performance forward osmosis membrane, Desalination 330 (2013) 70–78, https://doi.org/10.1016/j.desal.2013.09.028.
[48] S. Lim, M.J. Park, S. Phuntsho, L.D. Tijing, G.M. Nisola, W.-G. Shim, W.-J. Chung, H.K. Shon, Dual-layered nanocomposite substrate membrane based on polysulfone/graphene oxide for mitigating internal concentration polarization in forward osmosis, Polymer 110 (2017) 36–48, https://doi.org/10.1016/j.polymer.2016.12.066.
[49] X. Li, Z. Wang, X. Han, Y. Liu, C. Wang, F. Yan, J. Wang, Regulating the interfacial polymerization process toward high-performance polyamide thin-film composite reverse osmosis and nanofiltration membranes: a review, J. Membr. Sci. 640 (2021), https://doi.org/10.1016/j.memsci.2021.119765.
[50] X. Lv, E. Wang, S. Liu, L. Liu, Y. Yin, S. Li, B. Su, L. Han, Tannic acid reinforced interfacial polymerization fabrication of internally pressurized thin-film composite hollow fiber reverse osmosis membranes with high performance, Desalination 538 (2022), 115926, https://doi.org/10.1016/j.desal.2022.115926.

[51] X. Zhang, S. Xiong, C.-X. Liu, L. Shen, S.-L. Wang, W.-Z. Lang, Y. Wang, Smart TFC membrane for simulated textile wastewater concentration at elevated temperature enabled by thermal-responsive microgels, Desalination 500 (2021), 114870, https://doi.org/10.1016/j.desal.2020.114870.
[52] X. Cai, T. Lei, D. Sun, L. Lin, A critical analysis of the α, β and γ phases in poly (vinylidene fluoride) using FTIR, RSC Adv. 7 (25) (2017) 15382–15389, https://doi.org/10.1039/c7ra01267e.
[53] W. Yan, Z. Wang, J. Wu, S. Zhao, J. Wang, S. Wang, Enhancing the flux of brackish water TFC RO membrane by improving support surface porosity via a secondary pore-forming method, J. Membr. Sci. 498 (2016) 227–241, https://doi.org/10.1016/j.memsci.2015.10.029.
[54] J. Xu, H. Yan, Y. Zhang, G. Pan, Y. Liu, The morphology of fully-aromatic polyamide separation layer and its relationship with separation performance of TFC membranes, J. Membr. Sci. 541 (2017) 174–188, https://doi.org/10.1016/j.memsci.2017.06.057.
[55] C. Klaysom, S. Hermans, A. Gahlaut, S. Van Craenenbroeck, I.F.J. Vankelecom, Polyamide/Polyacrylonitrile (PA/PAN) thin film composite osmosis membranes: film optimization, characterization and performance evaluation, J. Membr. Sci. 445 (2013) 25–33, https://doi.org/10.1016/j.memsci.2013.05.037.
[56] S.-J. Park, S.J. Kwon, H.-E. Kwon, M.G. Shin, S.-H. Park, H. Park, Y.-I. Park, S.-E. Nam, J.-H. Lee, Aromatic solvent-assisted interfacial polymerization to prepare high performance thin film composite reverse osmosis membranes based on hydrophilic supports, Polymer 144 (2018) 159–167, https://doi.org/10.1016/j.polymer.2018.04.060.
[57] R.N. Wenzel, Resistance of solid surfaces to wetting by water, Ind. Eng. Chem. 28 (8) (1936) 988–994, https://doi.org/10.1021/ie50320a024.
[58] G. Hurwitz, G.R. Guillen, E.M.V. Hoek, Probing polyamide membrane surface charge, zeta potential, wettability, and hydrophilicity with contact angle measurements, J. Membr. Sci. 349 (1–2) (2010) 349–357, https://doi.org/10.1016/j.memsci.2009.11.063.
[59] Y. Zhao, M. Li, Q. Lu, Z.J.L. Shi, in: Superhydrophobic Polyimide Films With a Hierarchical Topography: Combined Replica Molding and Layer-by-layer Assembly 24(21), 2008, pp. 12651–12657.
[60] Y. Mansourpanah, K. Alizadeh, S.S. Madaeni, A. Rahimpour, H. Soltani Afarani, Using different surfactants for changing the properties of poly(piperazineamide) TFC nanofiltration membranes, Desalination 271 (1–3) (2011) 169–177, https://doi.org/10.1016/j.desal.2010.12.026.
[61] X. Yang, Controllable interfacial polymerization for nanofiltration membrane performance improvement by the polyphenol interlayer, ACS Omega 4 (9) (2019) 13824–13833, https://doi.org/10.1021/acsomega.9b01446.
[62] C. Li, S. Li, J. Zhang, C. Yang, B. Su, L. Han, X. Gao, Emerging sandwich-like reverse osmosis membrane with interfacial assembled covalent organic frameworks interlayer for highly-efficient desalination, J. Membr. Sci. 604 (2020), 118065, https://doi.org/10.1016/j.memsci.2020.118065.
[63] Z. Wang, P. Lu, G. Zhang, Y. Yong, C. Yang, Z.-S. Mao, Experimental investigation of marangoni effect in 1-hexanol/water system, Chem. Eng. Sci. 66 (12) (2011) 2883–2887, https://doi.org/10.1016/j.ces.2011.03.048.
[64] G. Duner, M. Kim, R.D. Tilton, S. Garoff, T.M. Przybycien, Effect of polyelectrolyte-surfactant complexation on marangoni transport at a liquid-liquid interface, J. Colloid. Interf. Sci. 467 (2016) 105–114, https://doi.org/10.1016/j.jcis.2016.01.011.
[65] N. Akther, Z. Yuan, Y. Chen, S. Lim, S. Phuntsho, N. Ghaffour, H. Matsuyama, H. Shon, Influence of graphene oxide lateral size on the properties and performances of forward osmosis membrane, Desalination 484 (2020), 114421, https://doi.org/10.1016/j.desal.2020.114421.
[66] Y. Li, Y. Zhao, E. Tian, Y. Ren, Preparation and characterization of novel forward osmosis membrane incorporated with sulfonated carbon nanotubes, RSC Adv. 8 (71) (2018) 41032–41039, https://doi.org/10.1039/c8ra08900k.
[67] Z. Shabani, T. Mohammadi, N. Kasiri, S. Sahebi, Thin-film nanocomposite forward osmosis membranes prepared on pvc substrates with polydopamine functionalized zr-based metal organic frameworks, Ind. Eng. Chem. Res. 61 (20) (2022) 7067–7079, https://doi.org/10.1021/acs.iecr.2c00874.
[68] D. Ma, S.B. Peh, G. Han, S.B. Chen, Thin-film nanocomposite (TFN) membranes incorporated with super-hydrophilic metal-organic framework (MOF) UiO-66: toward enhancement of water flux and salt rejection, ACS Appl. Mater. Interfaces 9 (8) (2017) 7523–7534, https://doi.org/10.1021/acsami.6b14223.
[69] L. Xu, J. Xu, B. Shan, X. Wang, C. Gao, Novel thin-film composite membranes via manipulating the synergistic interaction of dopamine and m-phenylenediamine for highly efficient forward osmosis desalination, J. Mater. Chem. A 5 (17) (2017) 7920–7932, https://doi.org/10.1039/c7ta00492c.
[70] S.J. Kwon, S.-H. Park, M.S. Park, J.S. Lee, J.-H. Lee, Highly permeable and mechanically durable forward osmosis membranes prepared using polyethylene lithium ion battery separators, J. Membr. Sci. 544 (2017) 213–220, https://doi.org/10.1016/j.memsci.2017.09.022.